

1 Phenotype prediction using biologically 2 interpretable neural networks on multi- 3 cohort multi-omics data 4

5 Arno van Hilten^{1*}, Jeroen van Rooij^{2*}, BIOS consortium, M. Arfan Ikram³, Wiro. J. Niessen^{1,4},
6 Joyce. B.J. van Meurs^{2,5}, Gennady V. Roshchupkin^{1,3}

7 ¹Department of Radiology and Nuclear Medicine, Erasmus MC, Rotterdam, The Netherlands

8 ²Department of Internal Medicine, Erasmus MC, Rotterdam, The Netherlands

9 ³Department of Epidemiology, Erasmus MC, Rotterdam, The Netherlands

10 ⁴Department of Imaging Physics, Delft University of Technology, Delft, The Netherlands

11 ⁵Department of Orthopaedics and Sports Medicine, Erasmus MC, Rotterdam, The Netherlands

12 * Contributed equally

16 Abstract

17 Integrating multi-omics data into predictive models has the potential to enhance accuracy, which is essential
18 for precision medicine. In this study, we developed interpretable predictive models for multi-omics data by
19 employing neural networks informed by prior biological knowledge, referred to as visible networks. These
20 neural networks offer insights into the decision-making process and can unveil novel perspectives on the
21 underlying biological mechanisms associated with traits and complex diseases. We tested the performance,
22 interpretability, and generalizability for inferring smoking status, subject age and LDL levels using genome-
23 wide RNA-expression and CpG methylation data from blood of the BIOS consortium(4 population cohorts,
24 N_total=2940). In a cohort-wise cross validation setting, the consistency of the diagnostic performance and
25 interpretation was assessed.

26 Performance was consistently high for predicting smoking status with an overall mean AUC of 0.95 (95% CI,
27 0.90 - 1.00) and interpretation revealed the involvement of well-replicated genes such as *AHRR*, *GPR15* and
28 *LRRN3*. LDL-level predictions only generalized in a single cohort with an R² of 0.07 (95% CI, 0.05 - 0.08). Age
29 was inferred with a mean error of 5.16 (95% CI, 3.97 - 6.35) years with the genes *COL11A2*, *AFAP1*, *OTUD7A*,
30 *PTPRN2*, *ADARB2* and *CD34* consistently predictive. In general, we found that using multi-omics networks
31 improved performance, stability and generalizability compared to interpretable single omic networks.

32 **We believe that visible neural networks have great potential for multi-omics analysis; they combine multi-**
33 **omic data elegantly, are interpretable, and generalize well to data from different cohorts.**

34

35 **Introduction**

36 Over the last decades, association studies have uncovered numerous genes and CpGs to be associated with
37 hundreds of traits and diseases¹. This has led to tools for identifying high risk individuals and biomarkers
38 for early disease detection. For example, blood-based methylation biomarkers are currently used for early
39 diagnosis for various forms of cancer^{2,3}. However, for most complex diseases and traits, the combined
40 effects, within and between different omics types, is still largely unexplored. For a more comprehensive
41 understanding of human health and diseases and for more accurate prediction models, it is therefore
42 necessary to study omic types in relation to one another. Thanks to recent technological improvements for
43 high throughput sequencing and arrays technologies, the acquisition of multi-omics datasets has become
44 more feasible, providing opportunities for new multi-omics analysis tools^{4,5}.

45

46 Recently, novel statistical frameworks and machine learning techniques have been published that integrate
47 multi-omics data in a single analysis^{6,7}. These studies show the potential for multi-omics analysis to
48 improve prediction for various disorders while providing insight into the disease biology^{4,8}. Integrating
49 different types of omics data in a single analysis is a challenging task, as each type has different,
50 procedures, preprocessing steps and analytical requirements⁹. Combining omics data presents additional
51 challenges, as each omic has unique dimensions, and it is essential to consider correlation structures both
52 within and between the different omics types. Thus, for the combined analysis of multiple omics types,
53 methods need to be flexible and be able to deal with the high dimensionality of these datasets.

54

55 Neural networks have demonstrated such flexibility and have been widely successful in fields such as
56 image classification¹⁰, speech recognition¹¹, and protein modelling¹². In contrast to most tasks in image
57 analysis and speech recognition, the focus of multi-omics frameworks is not only on predictive

58 performance but also in understanding the underlying etiology. To facilitate this, a new field in machine
59 learning, coined visible machine learning¹³ emerged, in which prior biological knowledge is embedded in
60 a neural network's architecture to create interpretable neural networks^{14–17}. Recent examples of these kinds
61 of neural networks applied in genomics are GenNet¹⁸ and P-net¹⁹. In the GenNet framework, gene and
62 pathway annotations were used to create interpretable neural networks for genetic risk prediction from
63 genotype. In P-net, methylation, gene expression and copy number variants were fed to an interpretable
64 neural network to differentiate between primary or metastatic prostate cancers. Other examples include,
65 PasNet²⁰, which integrated pathways information to predict survival for glioblastoma multiforme, a
66 primary brain cancer. DrugCell²¹ integrated Gene Ontology knowledge in a network to predict drug
67 response for various cancers and ParsVNN²² continued on this work and pruned the network for increased
68 performance and better interpretability.

69
70 In this study, we create visible neural networks to analyze multi-omics data in a single analysis. We
71 extend the GenNet framework to create interpretable neural networks for multiple omics inputs and apply
72 it to a dataset with transcriptomics and methylomics data. We validate the method using four cohorts in
73 the BIOS consortium for the application of predicting age, low-density lipoproteins (LDL) levels and
74 smoking status. Age prediction from methylation or gene expression data has been an active research area
75 popularized by the work of Hannum et al. and Horvath^{23,24}. Additionally, it has been shown that these
76 clocks show an asymptote for older participants and strong biological sex differences, making age
77 prediction particularly interesting to study with neural networks²⁵. Smoking status and LDL level
78 predictions are well-suited to evaluate the performance, stability and interpretation of the method.

79 Methylation and gene expression are highly predictive for smoking status and predictive genes are well-
80 documented^{26,27}. On the other hand, low lipid lipoprotein cholesterol levels is a complex outcome with
81 both environmental and genetic factors²⁸.

82 To summarize, we develop visible neural networks for multi-omics data and investigate their
83 generalizability and robustness for three different phenotypes by leveraging the multi-cohort setting of the

84 BIOS consortium in a cohort-wise cross validation analysis. Furthermore, we use the flexibility and
85 interpretability of these models to find sex-specific effects, omic-specific information and genes and
86 pathways important for prediction

87

88 **Materials & Methods**

89 **BIOS**

90 In this study, multi-omics data gathered by the Biobank-based Integrative Omics Study (BIOS)
91 consortium was used to predict smoking status, age and low-density lipoprotein levels. Specifically, we
92 used transcriptome and methylome data from BIOS four largest cohorts; LifeLines (LL), Leiden
93 Longevity Study (LLS), Netherlands Twin Register (NTR), and Rotterdam Study (RS). All cohorts within
94 the BIOS consortium followed the same procedure in gathering and processing data. For each participant,
95 transcriptome and the methylome were measured in whole blood samples taken from the same visit. DNA
96 methylation was profiled according to the manufacturer's protocol using the Infinium Illumina
97 HumanMethylation 450k arrays, while blood was first depleted from globin transcripts for RNA
98 sequencing. A detailed description of all data generation and preprocessing steps for the RNA sequencing
99 and DNA methylation data can be found in Zhernakova et al. (2017)²⁹ and Bonder et al. (2017)³⁰. Using
100 the BBMRI-NL's Integrative Omics analysis platform³¹, all individuals that had both RNA-seq and
101 methylation data (β -value) available were selected, resulting in a dataset with 2940 individuals. Y-
102 chromosomal data was excluded, X-chromosomal and autosomal measurements were included. Finally,
103 RNA-seq expression data was filtered using an expression inclusion criterion of one count per million on
104 average across all samples or higher⁹. An overview of the characteristics for each cohort can be found in
105 Table 1.

106

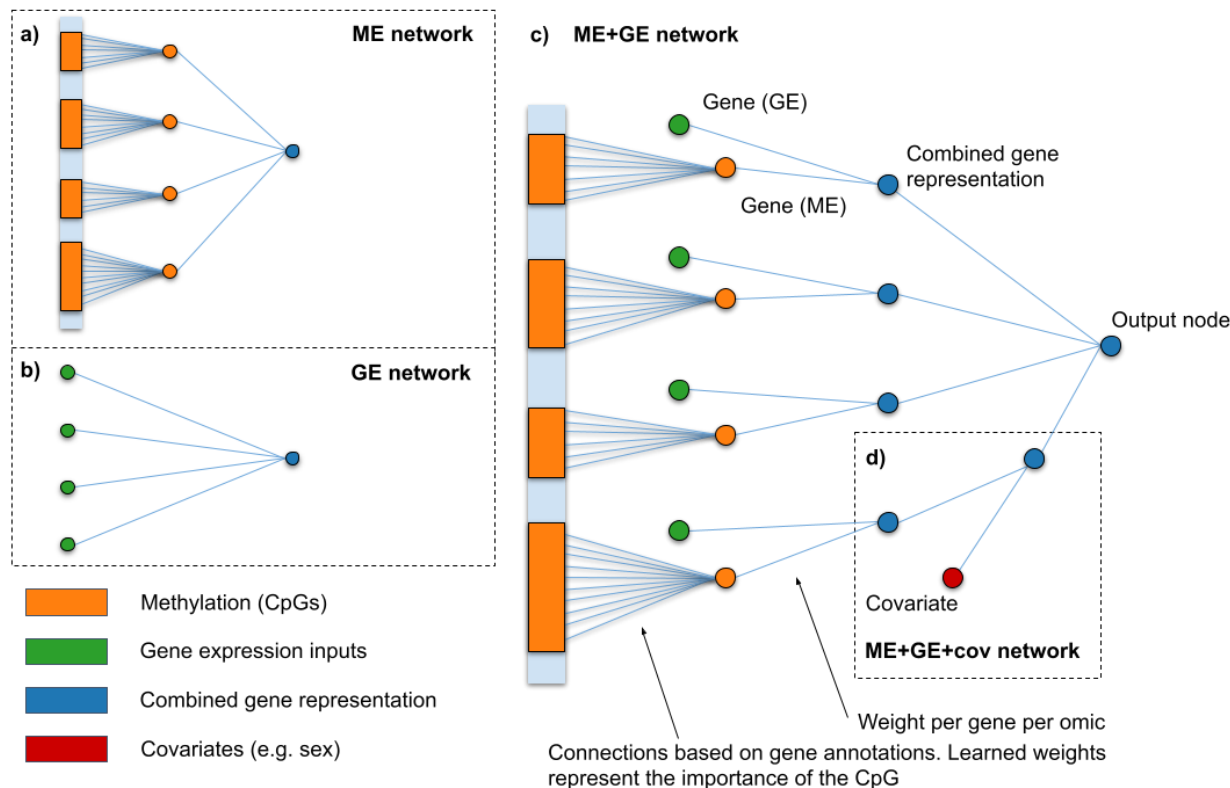
107

| | Rotterdam Study | LifeLines | Leiden Longevity Study | Netherlands Twin Register | Total of all cohorts |
|------------------------------------|--------------------|--------------------|------------------------|---------------------------|----------------------|
| Abbreviation | RS | LL | LLS | NTR | |
| Individuals | 693 | 727 | 646 | 874 | 2940 |
| Sex, male female | 397 296 | 421 306 | 340 306 | 577 297 | 1735 1205 |
| Smokers*, current never | 75 231 | 107 337 | 75 184 | 155 500 | 412 1252 |
| Age [years], mean + 95% CI | 67.6 (67.1 - 68.0) | 45.4 (44.4 - 46.3) | 58.8 (58.3 - 59.3) | 38.3 (37.3 - 39.3) | 51.4 (50.9 - 52.0) |
| LDL [mmol/L], mean + 95% CI | 3.32 (3.26 - 3.39) | 3.19 (3.12 - 3.25) | 3.36 (3.29 - 3.43) | 2.90 (2.84 - 2.96) | 3.17 (3.14 - 3.2) |

108
109
110 *Table 1. Main characteristics for all cohorts used in this study. Note the age differences between the cohorts; participants of the*
Netherlands Twin Register were on average 29 years younger than the participants of the Rotterdam Study. *Former smokers
were excluded in this study. CI; confidence interval.

111

112 **Network design**



113

114 *Figure 1. Schematic overview of the neural network architectures used in this study. In the ME network (a), DNA methylation*
115 *data (CpGs) are grouped and connected using gene annotations. The resulting 10,404 gene nodes are directly connected to the*

116 *output node. Combining the ME network and the the GE network (b) for gene expression, results in the ME+GE network (c). In*
117 *the ME+GE network each gene has a node per omic and a combined gene representation. Design (d) adds a covariate input to*
118 *the combined gene representation for each gene. This allows the ME+GE network to model gene-specific effects for the covariate.*
119 *A schematic overview of the pathway network and a similar fully connected network can be found in Supplementary Figure 1.*

120 Neural network architectures were created using principles from the GenNet framework¹⁸. This
121 framework uses prior knowledge (e.g., gene and pathway annotations) to connect input data to the neurons
122 in the next layer of neural network. CpG methylation sites were annotated using GREAT³² (Genomic
123 Regions Enrichment of Annotations Tool) and connected to the closest gene based on genomic distance
124 (in base pairs) resulting in 17,283 gene annotations for 481,388 methylation sites. These gene annotations
125 were intersected with the 14,248 remaining gene expression measurements left after preprocessing,
126 resulting in an overlap of 10,404 genes between both omic types. This set of overlapping genes was used
127 in all analyses. The methylation gene layer was built using these genes and their corresponding 324,295
128 CpGs. For the creation of pathway layers the set of overlapping genes was grouped into KEGG's
129 functional pathways³³ from ConsensusPathDB³⁴. Out of the 10,404 genes, 4813 genes were annotated for
130 at least one pathway.

131 The gene expression network (GE network, Figure 1a) is the simplest network and consists of the gene
132 expression input connected straight to the output node similar as in LASSO regression. The methylation
133 network (ME network, Figure 1b) which consists of the input methylation data, a gene layer with neurons
134 representing gene methylation made and an output node. The methylation and gene expression network
135 (ME + GE network, Figure 1c) combines both networks. In a similar way as in the ME network, CpGs are
136 fed to the first layer of the network and reduced to one node per gene using gene annotations. In contrast
137 to most other methods, gene expression is not concatenated to the input but used as a separate input in the
138 gene level of the network. In this layer, gene expression is combined with the neurons representing genes
139 by methylation. Finally, a single node was used to predict the target phenotype.

140 The activation function transforms the output signal for each neuron. For classification tasks, such as
141 predicting if an individual smokes or not, a sigmoid activation function was used to scale the output to the
142 range [0, 1] in the last neuron. Arctanh activation functions were used for all other layers to introduce non-

143 linearities, increasing the modelling capabilities of the network. For regression tasks, such as predicting
144 continues traits such as age and LDL levels, ReLu activation functions with output range $[0, \infty)$ were used
145 for all layers. For a better initialization of the network, the bias of the last neuron was set to the mean
146 value of the predicted outcome in the training set.

147 **Deeper networks**

148 For more complex modelling of the interactions between expression, methylation and phenotypes, we also
149 evaluated deeper networks (Supplementary Figure 1). First, using KEGG's functional pathways^{33,34} as
150 prior knowledge, three hierarchical pathway layers were created. The first layer groups genes into 321
151 functional pathways such as: *insulin secretion*, *thyroid hormone synthesis* and *PPAR signaling pathway*.
152 The forementioned pathways are all part of the endocrine system group which, in turn, is a subgroup of
153 organismal systems. The mid and global-level pathway layers were created adopting this hierarchical
154 structure, consisting of 44 and 6 groups, respectively. Each pathway is represented by its own neuron
155 resulting in three layers with 321, 44 and 6 nodes each. Not all genes were annotated by the KEGG
156 functional pathway annotations, 5591 genes did not receive a functional pathway annotation. To ensure
157 connectivity to the output for all genes, connections that skip the pathway layers (skip connections) were
158 added from each gene to the output node.

159 Additionally, a deeper network was constructed without any additional prior biological knowledge to
160 compare with the KEGG pathway network. Similarly, the ME+GE network served as a basis for this
161 network and three densely connected layers, 321, 44 and 6 nodes each, were added between the gene layer
162 and the output node. The resulting network has thus the same number of neurons as the KEGG pathway
163 network, but has fully connected layers instead of layers based on KEGG pathway information.

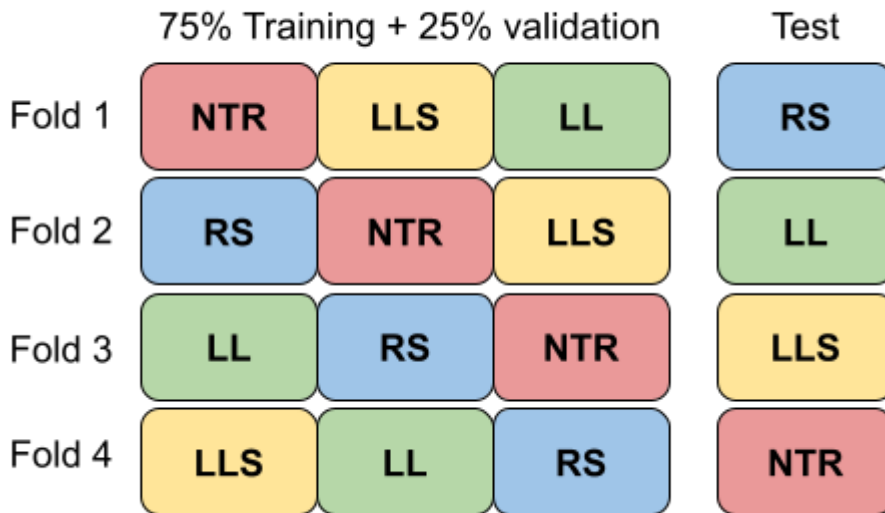
164 **Training and evaluation**

165 The neural networks were evaluated in a cohort-wise cross validation setup as shown in Figure 2 to assess
166 the generalizability of the models across cohorts. Each fold, one cohort is held out as test set, while the
167 three other cohorts were used for training and validation (leave-one-out method). From these three cohorts

168 75% of the individuals were randomly selected for the training set while the remaining 25% was used in
169 the validation set to tune the hyperparameters. For all methods the same combinations of hyperparameters
170 were tuned on the validation set. Combinations included learning rates of [0.01, 0.001, 0.005, 0.0001] and
171 L1 penalty on the weights of the combined gene and/or methylation gene layer of [0.01, 0.001, 0.0001]. A
172 higher L1 penalty increases the cost for the network to include more contributors to predict the outcome.
173 The L1 penalty thus enforces sparsity over the weights, so that most inputs get assigned a (near) zero
174 weight while important inputs still get assigned a high weight. This L1 regularization on the weights helps
175 preventing overfitting and increases interpretability.

176 The mean squared error (MSE) was used as a loss function to optimize for regression tasks. For
177 classification tasks, weighted binary cross entropy, with a weight inverse to the ratio of the class
178 imbalance, was used as a loss function. The loss function quantifies the difference between current
179 outcome and the true label and is optimized during training. The performance of the resulting network is
180 evaluated using the area under the receiver operating curve (AUC) for classification tasks, and the root
181 mean squared error (RMSE) and explained variance for regression tasks (explained variance can be found
182 in the Supplementary Materials). For each fold the hyperparameters of the best performing model in the
183 validation set were selected to evaluate on the test cohort. Since neural networks use stochastic processes
184 that can influence the outcome, we trained the network with the best hyperparameters ten times with a
185 different random seed to investigate its stability.

Cohort-wise cross validation



186
187 *Figure 2. Cohort-wise cross-validation. For each fold three cohorts were used to train and validate the hyperparameters of the*
188 *model (75% training, 25% validation). The remaining, left-out cohort served as an independent test set and the average*
189 *performance over the test cohorts was reported. The cohort-wise cross validation was done for each phenotype (smoking, LDL*
190 *and age prediction). Abbreviations: Netherlands Twin Register (NTR), Leiden Longevity Study (LLS), LifeLines (LL), Rotterdam*
191 *Study (RS).*

192 Additional analyses

193 Neural networks are flexible methods and with the inclusion of prior biological knowledge different
194 architectures can be explored to provide more insight into the interaction between omics types,
195 contribution of covariates and gene-specific contribution of covariates. For each of these analyses we
196 made small changes to the ME+GE networks.

197 *Omic-specific information*

198 Gene expression and methylation data contain redundant information with respect to each other. However,
199 not all information that is present in the one may be present in the other data type. To evaluate the
200 independent contribution of each omics to the prediction we add a L1 penalty for one omics type in the
201 model. This introduces a trade-off for the neural network: the gain in performance for including
202 information of the penalized omic (i.e., RNA expression of a single gene or the methylation representation
203 of a single gene) must outweigh its penalty. If the model uses only the non-penalized omic type without
204 loss of prediction performance, it is likely that there was no omic-specific information. However, if the

205 model still decides to use parts of the penalized omics data, this information is most likely unique to the
206 penalized omic type and was therefore required for prediction.

207 *Covariate-gene interaction*

208 Including covariates in the model, for example sex and age for smoking, can improve performance and
209 interpretation. Commonly, the covariates are included as an extra layer at the end. However, by adding a
210 covariate for each gene, more specific information in how a covariate affects a single gene can be obtained
211 (see Figure 1d). For each phenotype we tested both, a model with covariates in the last layer and a model
212 with covariates for each gene.

213 *Subtyping with activation patterns*

214 In contrast to fully-connected neural networks, the visible neural network architectures used in this study
215 are constructed based on prior biological knowledge can be interpreted by inspecting the weights of the
216 incoming and outgoing connections. The strength of the weights (e.g., between CpGs and genes,
217 expression and genes, genes and pathways), all express the importance of these biological elements for the
218 predicted outcome. The weights of a neural network are a result of an optimization over the population it
219 was trained on, and are thus a result of the population characteristics of the training set. However, neural
220 networks may learn different patterns for the same outcome. By inspecting the weights general
221 information is learned about the importance of each element but this does not show differences between
222 groups or individuals. Based on differences between individuals, some neurons can activate for a certain
223 group of individuals, while it does not for others. To gain an overview of the different patterns that are
224 learned by the network we applied principal component analysis³⁵ (PCA) over all the activations for all
225 (gene-level) nodes for each individual. In this PCA, individual-level differences may cluster and provide
226 groups of individuals for which the neural network used a similar activation pattern.

227

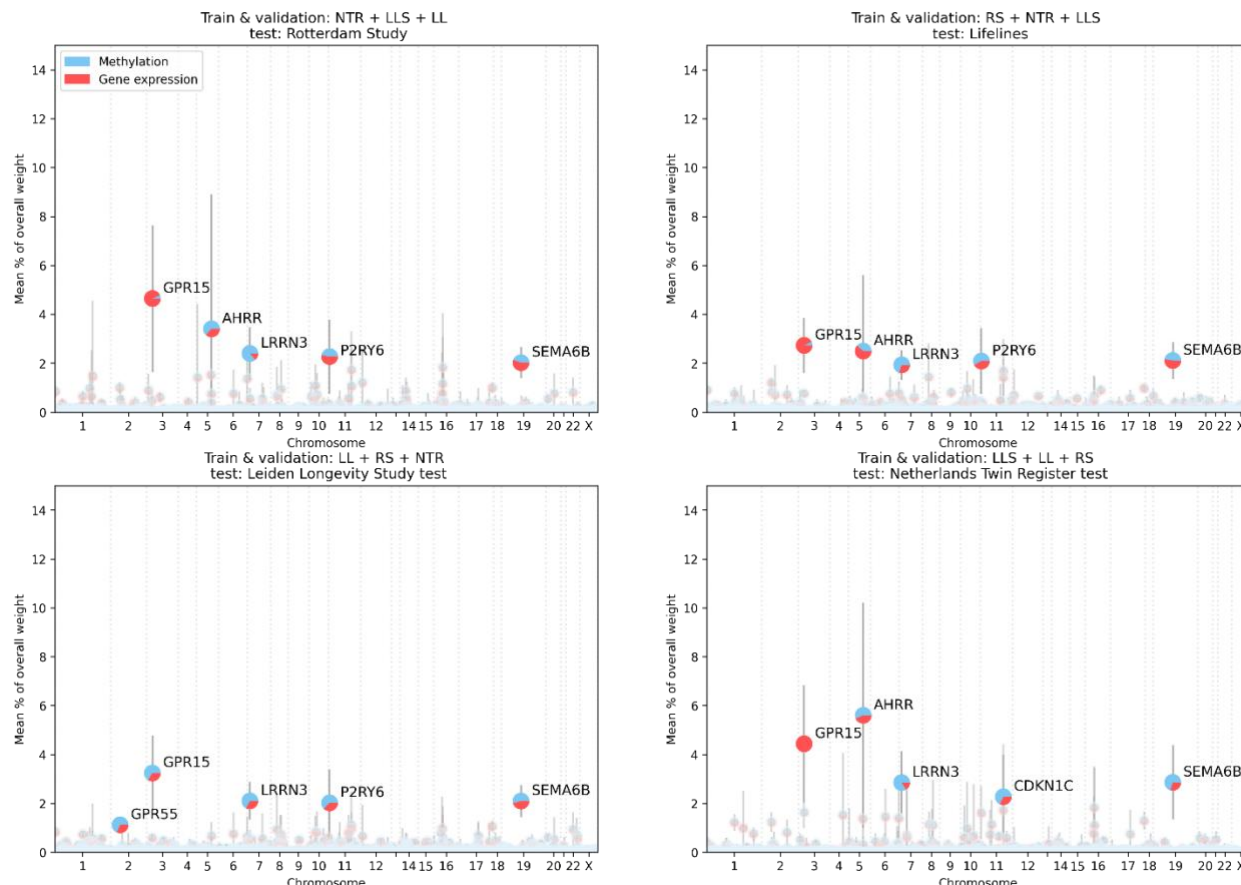
228 **Results**

| Phenotype | Network type | AUC validation cohorts | | | | AUC test cohort | | | | Mean test AUC over all cohorts |
|-----------|--------------|--------------------------|-----------------------|--------------------------|-------------------------|-------------------------|--------------------------|------------------------|--------------------------|---------------------------------|
| | | RS* | LL* | LLS* | NTR* | RS | LL | LLS | NTR | |
| Smoking | ME+GE | 0.92 (0.90 - 0.94) | 0.93 (0.92 - 0.93) | 0.91 (0.90 - 0.92) | 0.93 (0.91 - 0.94) | 0.98 (0.98 - 0.98) | 0.92 (0.92 - 0.93) | 0.95 (0.95 - 0.96) | 0.91 (0.89 - 0.92) | 0.95 (0.90 - 1.00) |
| | ME | 0.93 (0.92 - 0.94) | 0.94 (0.94 - 0.95) | 0.95 (0.94 - 0.95) | 0.93 (0.93 - 0.94) | 0.97 (0.97 - 0.98) | 0.94 (0.93 - 0.94) | 0.96 (0.95 - 0.96) | 0.95 (0.95 - 0.96) | 0.95 (0.93 - 0.98) |
| | GE | 0.83 (0.83 - 0.84) | 0.82 (0.82 - 0.82) | 0.83 (0.83 - 0.83) | 0.87 (0.86 - 0.87) | 0.87 (0.87 - 0.88) | 0.85 (0.85 - 0.85) | 0.87 (0.87 - 0.88) | 0.80 (0.80 - 0.80) | 0.85 (0.80 - 0.90) |
| Phenotype | Network type | RMSE validation cohorts | | | | RMSE test cohorts | | | | Mean test RSME over all cohorts |
| | | RS* | LL* | LLS* | NTR* | RS | LL | LLS | NTR | |
| Age | ME+GE | 3.85 (3.72 - 3.98) | 4.13 (4.03 - 4.23) | 3.88 (3.78 - 3.98) | 4.12 (3.99 - 4.25) | 5.44 (5.23 - 5.65) | 6.04 (5.76 - 6.31) | 4.20 (4.11 - 4.29) | 6.33 (5.87 - 6.8) | 5.16 (3.97 - 6.35) |
| | ME | 14.48 (13.04 - 15.92) | 8.23 (7.26 - 9.19) | 18.06 (15.01 - 21.11) | 11.28 (9.90 - 12.66) | 15.69 (12.37 - 19.0) | 8.14 (6.50 - 9.79) | 13.17 (9.13 - 17.2) | 22.66 (19.67 - 25.65) | 15.00 (4.31 - 25.69) |
| | GE | 6.79 (6.77 - 6.81) | 6.52 (6.51 - 6.53) | 6.40 (6.38 - 6.41) | 6.16 (6.14 - 6.17) | 9.03 (8.80 - 9.26) | 12.23 (12.04 - 12.41) | 6.87 (6.80 - 6.95) | 17.77 (17.51 - 18.03) | 11.45 (4.21 - 18.68) |
| LDL | ME+GE | 0.88 (0.87 - 0.88) | 0.88 (0.88 - 0.88) | 0.85 (0.84 - 0.86) | 0.92 (0.91 - 0.92) | 0.92 (0.92 - 0.93) | 0.89 (0.89 - 0.90) | 0.93 (0.93 - 0.94) | 0.93 (0.91 - 0.95) | 0.93 (0.88 - 0.99) |
| | ME | 1.18 (1.12 - 1.25) | 1.14 (1.06 - 1.22) | 1.10 (1.02 - 1.18) | 1.12 (1.08 - 1.16) | 1.29 (1.15 - 1.44) | 1.17 (1.07 - 1.26) | 1.10 (1.01 - 1.19) | 1.23 (1.15 - 1.30) | 1.27 (0.8 - 1.75) |
| | GE | 0.88 (0.88 - 0.88) | 0.88 (0.88 - 0.89) | 0.85 (0.85 - 0.86) | 0.90 (0.90 - 0.91) | 0.94 (0.93 - 0.94) | 0.90 (0.89 - 0.90) | 0.93 (0.93 - 0.93) | 1.02 (0.98 - 1.07) | 0.98 (0.79 - 1.17) |

229 *Table 1. Performance for cohort-wise cross validation, mean with 95% confidence interval over 10 runs. The area under the curve*
230 *is reported for the classification task (smoking status prediction) and the root mean squared error (RMSE) for the regression*
231 *tasks; predicting age and LDL levels. ME; Methylation, GE; Gene expression, ME+GE, both methylation and gene expression*
232 *as an input for the neural network. RS; Rotterdam study, LL; LifeLines, NTR; Netherlands Twin Register, LLS; Leiden Longevity*
233 *Study. See Supplementary Table 1 for the performance of out-of-the-box scikit-learn implementations for each omic. *The name of*
234 *the test cohort is used to denote the fold. Thus, for the first fold, RS, was used for testing and LL+LLS+NTR were used for*
235 *training and validation (75% training, 25% validation).*

236

Interpretation: gene contribution for predicting smoking status in the cohort-wise cross validation



237
 238 *Figure 3. Overview of the important genes for predicting smoking status for each fold. Contribution was measured in percentage*
 239 *of the total weight assigned to each gene. For each gene, the pie chart shows the contribution of methylation and gene expression.*
 240 *Error bars indicate the standard deviation over ten runs for the exact same network trained with the same hyperparameters.*

241 **Cohort-wise cross validation**

242 An overview of the performance for each cohort and for the three different architectures can be found in
 243 Table 2. It shows the mean predictive performance and standard deviation for each fold for ten networks
 244 trained with the same hyperparameters but with different random seeds. The corresponding
 245 hyperparameters, chosen on the best performance in the validation set, can be found in Supplementary
 246 Table 2.

247 *Predicting smoking status*

248 Both gene expression and methylation were highly predictive for smoking status in all folds. The best
 249 performance was achieved by the ME+GE network, thus with both methylation and gene expression input,
 250 in the fold with the Rotterdam Study as test cohort (all other cohorts were used for training and

251 validation). In this fold, the network achieved a near perfect classification with area under the receiver
252 operating curve (AUC) of 0.98 (95% confidence interval, 0.98 - 0.98). Over all folds, the ME networks
253 and ME+GE networks performed best with a mean AUC of 0.95 (95% CI, 0.93 - 0.98) and 0.95 (95% CI,
254 0.90 - 1.00) respectively. The GE network, based solely on gene expression input, performed substantially
255 worse with a mean AUC of 0. 0.85 (95% CI, 0.80 - 0.90). Surprisingly, the mean test performance over all
256 folds for the ME+GE network was lower for deeper networks with three fully connected layers, achieving
257 a mean AUC of 0.91 (95% CI, 0.85 - 0.96) (see Supplementary Table 3). In general, each fold obtained
258 good predictive performance for predicting smoking status, the GE network in the fold with NTR as test
259 cohort achieved the worst overall predictive performance with a mean AUC of 0.80 (95% CI, 0.80 - 0.80).
260 The ME+GE networks exhibit a stable performance, with small confidence intervals for the area under the
261 curve and standard deviations not exceeding 0.03. However, there may be significant variations in the
262 underlying weights due to stochastic processes used for network initialization and training, resulting in
263 different starting points and optimization paths for all weights across runs. As the weights within a neural
264 network operate relative to each other and cannot be directly compared between networks, we compared
265 the relative contribution of each gene instead. Figure 3 demonstrates that certain genes are consistently
266 utilized by the network to differentiate between current smokers and non-smokers across all folds,
267 although there can be notable differences in the percentage of total weight each gene holds. In each fold,
268 *GPR15* is the most or second most predictive gene for smoking status, its signal is mainly driven by gene
269 expression as visualized in Figure 3. Specifically, $79.8 \pm 33.3\%$ (mean and standard deviation over all
270 folds) of the weights that drive the signal for this gene are from the gene expression input. The next gene,
271 *AHRR*, is important for prediction in three out of four cohorts. This signal is driven by both gene
272 expression (44.3%) as well as methylation (55.6%). Other consistently highly predictive genes (i.e., genes
273 with a weight contribution higher than 1% in three out of four cohorts) are *SEMA6B*, *PID1*, *LRRN3*,
274 *P2RY6*, *CDKN1C*, *CLEC10A* and *KCNQ1*. (See Supplementary Table 4 for more details). All these
275 consistently highly predictive genes were found before in association studies for smoking in gene

276 expression and methylation³⁶⁻³⁸. A graphical overview of important pathways for smoking prediction can
277 be found in Supplementary Figure 2.

278 To investigate the interplay between the omic types, two additional analyses were conducted where either
279 gene expression or methylation gene representations were penalized (see Supplementary Figures 3,4 and
280 5). Without penalization the weights for gene expression and methylation were nearly equally divided
281 after training. Weights connected to gene expression input occupied $51.6 \pm 1.3\%$ of the weights over all
282 the ME+GE networks, the remainder used for methylation. In these experiments, we found that an omic
283 specific L1 penalty of 0.01 for gene expression reduced the contribution of the weights associated with
284 gene expression to $0.69 \pm 1.16\%$ while a similar threshold reduced the weights associated with
285 methylation to $2.56 \pm 1.73\%$. A more severe omic specific L1 threshold of 0.001 for methylation reduced
286 the use of methylation in the top genes nearly completely, only for *LRNN3* methylation input is still used
287 in the second and third fold with (respectively ~41% and 16% of the weights for this gene). However, with
288 the same threshold gene expression inputs are responsible for 15% of the weights for AHRR in the first
289 fold, nearly 29% of the *GPR15* weights in the second fold and 39% of *RER1* in the fourth fold (see **Error!**
290 **Reference source not found.** and 4). Interestingly, the importance of AHRR was severely impacted by
291 the methylation penalty, its gene expression was barely used to predict smoking status when methylation
292 was penalized.

293 ***Predicting age***

294 Networks trained with both methylation and gene expression data (ME+GE) achieved a mean error of
295 5.16 (95% CI, 3.97 - 6.35) years over all folds for age prediction (see Table 1). Between folds, there were
296 large differences in performance for predicting age. Most notably, networks did not generalize well in
297 folds that have either the Rotterdam Study (ranging between 52 to 80 years) or the Leiden Longevity
298 Study (ranging between 30 to 79 years) as test cohort, the two cohorts with the oldest population. For
299 these cohorts, the explained variance in the test set was substantially lower than in the validation set:
300 Rotterdam study test 0.40 (95% CI, 0.37 - 0.43), 0.94 (95% CI 0.93 - 0.94) validation, Leiden Longevity

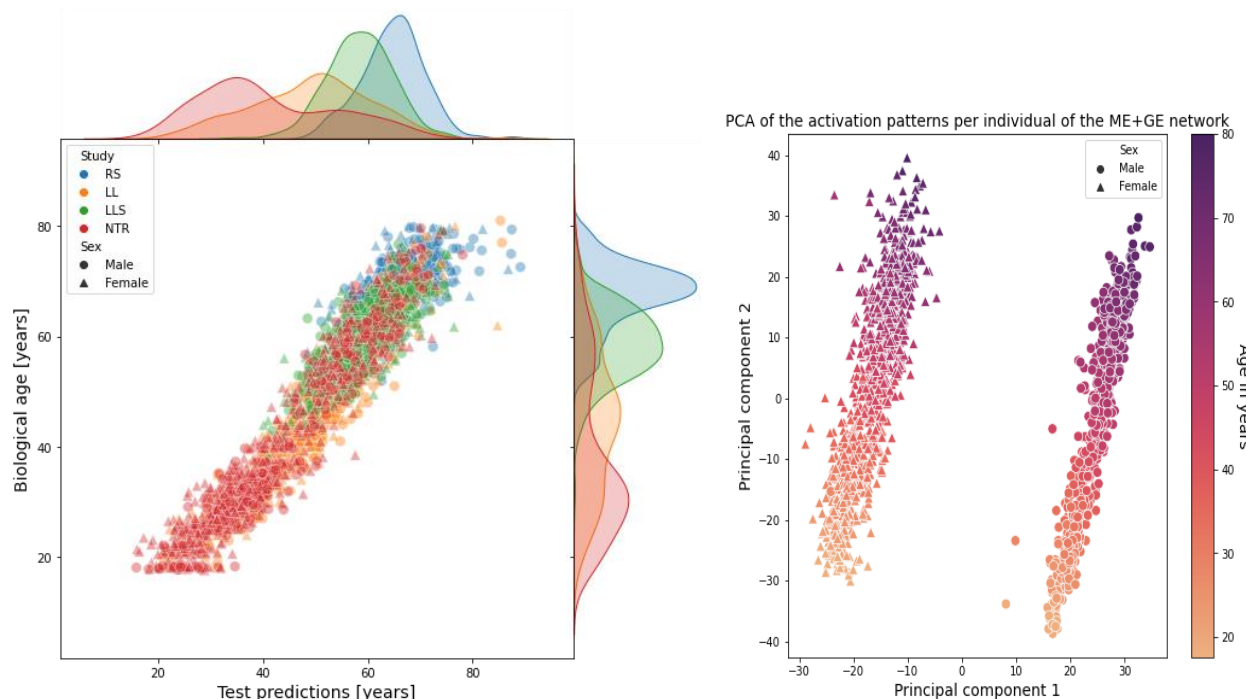
301 Study test 0.95 (95% CI, 0.95 - 0.95), 0.61 (95% CI, 0.60 - 0.63) validation. Aside from being older, these
302 cohorts also have a smaller spread in age distribution compared to the two other cohorts (See Figure 4a
303 and Supplementary Figure 6). The Netherlands Twin Register cohort ranges between roughly 18 and 80
304 years old while individuals from the Lifelines cohort were between 18 and 81 years old.

305 Differences between omics and network types were also larger for age prediction than for smoking status
306 prediction. The ME+GE network consistently outperformed the single-omic networks with substantial
307 margins: the mean explained variance over all folds was 0.72 (95% CI, 0.36 - 1.07) for the ME+GE
308 network, 0.30 (95% CI, -0.26 - 0.86) for gene expression, while the ME networks did not find any
309 predictive pattern that translated to the test cohort. Training and validation performance was generally
310 poor for the ME network, and although the GE network obtained good validation performance in terms of
311 explained variance for each fold, this did not translate in folds with the Rotterdam study and Leiden
312 Longevity Study as test cohorts.

313 Interpretation of the ME+GE network revealed that many genes had a small contribution for age
314 prediction (see Supplementary Figure 6). The neural network found a more multifactorial solution for age
315 prediction than for smoking, the most important gene over all folds only occupied 0.68% of all weights for
316 predicting age compared to 3.76% for smoking. The most predictive genes with a weight contribution
317 higher than 0.30% of the total weight in three out of the four folds were *COL11A2*, *AFAP1*, *OTUD7A*,
318 *PTPRN2*, *ADARB2* and *CD34* (Supplementary Table 5). These most predictive genes were not part of
319 Hannum et al. and Horvath's epigenetic clocks^{23,24}.

320 The first principal components of the activation patterns of the ME+GE network revealed distinct
321 activation patterns for the different sexes with a gradient in each cluster (see 4b). Although, there is no
322 significant difference in the absolute error between the sexes (Wilcoxon rank-sum, p-value of 0.98,
323 Supplementary Figure 7,8), the first principal component clusters perfectly for males and females while
324 the second principal component is strongly related with age. Additional experiments showed that the
325 clustering of the sexes is mainly driven by genes on the X chromosome (see Supplementary Figure 9).

326 Including sex as a covariate in the last layer of the model did not improve the performance of the model
327 (mean RMSE over all folds of 7.31 [95% CI, 2.89 - 11.73]). Including sex information to each gene also
328 did not lead to a better performance (mean RMSE over all folds of 10.64 [95% CI, 4.12 - 17.15]).
329 However, inspecting the weights between the covariate and the genes for the best performing network
330 revealed strong sex-specific weights for, among others: *KLF13*, *ANO9* and *HECA* (for more details see
331 Supplementary Figure 10). For these genes the network needed strong weights to model sex-specific
332 effects for age prediction.



333
334 *Figure 4. a) Test predictions for the ME+GE network for all folds (each cohort) with corresponding distributions (See*
335 *Supplementary 11 and 12 for the GE and ME networks). b) Activation of the ME+GE trained for age prediction. A principal*
336 *component analysis clearly shows two distinct activation patterns corresponding to the different sexes. Principal component 1 is*
337 *related to the sex differences, principal component 2 to the age of the participants.*

338 After applying an omic-specific L1 penalty for methylation of 0.01, the network only used the methylation
339 input for gene *NEDD1* in the second fold with nearly 33% of the weight contribution for this gene from
340 methylation, while in the third fold *MAD1L1* had a methylation contribution of 23% (see Supplementary
341 Figure 14). With the same threshold for penalizing gene expression inputs, *DNAJB6* had the largest gene

342 expression use with 31% of the weight for this gene assigned to gene expression input (Supplementary
343 Figure 15). The deeper neural network architectures quickly overfitted, reaching high performance on the
344 training data which did not generalize to the validation and test set. These networks were consistently
345 outperformed by the ME+GE network (Supplementary Table 5). The best performing network build with
346 KEGG pathway information had the pathway: “environmental information processing” as the most
347 predictive global pathway because of high contributions of membrane transport (ABC transporters), signal
348 transduction, and signaling molecules and interaction (see Supplementary Figure 16).

349 *Predicting low-density lipoproteins levels*

350 ME+GE and GE networks explained up to 17% of the phenotypic variance in the validation set but these
351 networks only generalized in the second fold to an explained variance of 0.07 (95% CI, 0.05 - 0.08) for the
352 ME+GE network and 0.04 (95% CI, 0.04 - 0.05) for the GE network in the Lifelines test cohort (see
353 **Error! Reference source not found.**). In this fold, the largest gene, *FAM53A* only occupied 0.052% of
354 the total weight (Supplementary Figure 17). The weights for all genes in the ME+GE network were small
355 and evenly spread, indicating that the network did not find individual genes with a strong effect for
356 predicting low-density lipoproteins levels. Additional layers, be it pathways or densely connected layers,
357 did not improve predictive performance.

358

359 **Discussion**

360 In this paper we evaluated the performance, interpretability and stability of visible neural networks for
361 single and multi-omics data. Interpretability was achieved by embedding prior biological knowledge such
362 as gene and pathway annotations in the neural network architecture. We applied these models to predict
363 smoking status, age and low-density lipoprotein levels in a cohort-wise cross validation using methylation
364 and gene expression data.

366

367 For smoking, single omic networks and multi-omic networks performed consistently high across all

368 cohorts for predicting smoking status. Predicting smoking status is a relatively simple task, since smoking
369 is a powerful inducer of DNA methylation and gene expression alterations³⁹. This is also reflected by the
370 mean AUC of 0.95 over all folds that the ME+GE and ME networks achieved. It is slightly better than the
371 performance of Maas et al. who reported an AUC of 0.90 in an external dataset with a weighted
372 combination of just thirteen CpGs. Inspection of the weights of the ME+GE network revealed *GPR15*,
373 *AHRR* and *LRRN3* as most important genes for prediction, which is consistent with existing
374 literature^{26,27,39,40}. In the ME+GE network the contribution of both omics types was nearly equal (in terms
375 of weights), while the gene expression-based network by itself was less predictive than the methylation-
376 based networks. Applying an omic-specific penalty for methylation input showed that the ME+GE
377 network needed some methylation input to achieve similar performance with expression information.
378

379 For predicting age, the ME+GE network outperformed the single ME or GE networks. The performance
380 of this network in the test cohorts varied between a R^2 of 0.40 (95% CI, 0.37 - 0.43) and 0.91 (95% CI,
381 0.90 - 0.92). This difference in performance is probably caused by the different distributions in age in the
382 cohorts, depending on the cohorts in the training set the networks are shown less examples of older or
383 younger individuals. Similar effect were also seen in traditional methods⁹. Based on the predictive
384 performance shown in Table 2 one could conclude that for age prediction, usage of the two omics types
385 increased stability and performance for these type of neural networks compared to the single omic
386 networks. Additionally, we have evaluated whether the network used sex-information in the decision
387 process for age prediction. The first principal component of the activations of the neural network showed a
388 perfect separation between the sexes, mostly caused by genes on the X-chromosome, while the second
389 principal component had a clear correlation with age. Owing to the shallowness of the networks, the
390 activation pattern will therefore closely resemble the underlying data, especially if it has some relation
391 with the outcome. For deeper networks a PCA on the activation may reveal more detailed information
392 (such as different patients subtypes or mediating factors) since the network applies more complex
393 transformations to the data. The inclusion of genes on the X-chromosome allowed the network thus to

394 separate between the sexes but it did not have the capacity to model different effects independently from
395 the input for each sex. To help the model to find a sex-specific effect we modified the network with sex
396 information as an extra input to each gene node. After, training the network found the strongest sex-
397 specific gene effects for *KL13*, *ANO9* and *HECA*. However, this addition to the network architecture did
398 not improve performance.

399

400 An earlier EWAS in only the Rotterdam study did not find significant associations between DNA
401 methylation in blood and low-density lipoproteins cholesterol⁴¹. Another EWAS using BIOS data found
402 only three significant associations, demonstrating that there is a very weak relation between methylation
403 and LDL measurements from blood which makes the prediction task more complex⁴². The neural
404 networks did find patterns in the training set that were also found in the validation set (up to an R^2 of 0.17
405 [95% CI, 0.16 - 0.18]) but this pattern did not generalize to the test cohorts with the exception of the
406 Lifeline cohort. In this cohort the method achieved an R^2 of 0.07 (95% CI, 0.05 - 0.08) in the test set,
407 substantially lower than the performance of the validation set 0.13 (95% CI, 0.12 - 0.14). suggesting that
408 the model had trouble generalizing to data from an unseen cohort. Overall, the low prediction performance
409 might also indicates that the studied omic-data (gene expression and methylation from blood) might not
410 contain enough information to accurately predict LDL-levels.

411 In general, we found that including multiple omics inputs in the network improved performance. These
412 multi-omic networks had a more stable performance and generalized better to the test cohorts.
413 Surprisingly, deeper networks did not lead to better performance. Generally, one would expect deeper
414 networks to perform better since they can model more complex interactions. Thus, it is possible that the
415 optimal hyperparameter values for deeper networks lie outside the considered hyperparameter range or
416 that more training examples are required to train these deeper networks. Interpreting the ME+GE networks
417 revealed well-known genes such as *GPR15* and *AHRR* for smoking that validate the results. However we
418 also saw that the interpretation can vary between different random initializations and it is therefore

419 recommended to train networks with different random seeds for a more complete overview of important
420 predictors. As for all prediction models, it is important to consider that predictive genes and pathways
421 found are not necessarily causal genes and pathways as effects can be mediated. However, these genes and
422 pathways do provide insight in the decision process of the neural network and may be used in follow-up.

423

424 For good interpretation, proper regularization is important as it forces the network to use the most
425 predictive input features. For example, an L1 penalty on the weights will force the network to learn sparse
426 weights, resulting in a less complex model. In the absence of an L1 penalty on the weights, the network
427 has more freedom to choose its weights. This does not necessarily harm performance, but may harm
428 interpretability. In this work we use the L1 penalty to regularize the network, but other regularization
429 methods could have been chosen. For example dropout⁴³, this method drives the network to find a more
430 stable solution by deactivating random sets of neurons during training. Another important factor for
431 interpretation in visible neural networks is the quality of the prior knowledge used in creation. In this
432 study, the annotations for the CpG sites were based on genomic distance. Potential improvements could
433 come from using tissue specific and functional annotation databases such as ENCODE⁴⁴

434

435

436 Conclusion

437
438 We believe that visible neural networks have great potential for genomic applications, especially for
439 multi-omics integration. These interpretable neural networks can combine multi-omics data elegantly in a
440 single prediction model and provide the importance of each gene, pathway and omic input for prediction.
441 Additionally, we found that using multi-omic networks generally improved performance, stability and
442 generalizability compared to interpretable single omic networks.

443

444

445

446 References

447

448 1. Li, M. *et al.* EWAS Atlas: A curated knowledgebase of epigenome-wide association studies.
449 *Nucleic Acids Res.* **47**, D983–D988 (2019).

450 2. Mikeska, T. & Craig, J. M. DNA methylation biomarkers: Cancer and beyond. *Genes (Basel)*. **5**,
451 821–864 (2014).

452 3. Taryma-Leśniak, O., Sokolowska, K. E. & Wojdacz, T. K. Current status of development of
453 methylation biomarkers for in vitro diagnostic IVD applications (Clinical Epigenetics
454 (2020)12:100Ddoi:10.1186/s13148-020-00886-6). *Clin. Epigenetics* **12**, 1–16 (2020).

455 4. Hasin, Y., Seldin, M. & Lusis, A. Multi-omics approaches to disease. *Genome Biol.* **18**, 1–15
456 (2017).

457 5. Ritchie, M. D., Holzinger, E. R., Li, R., Pendergrass, S. A. & Kim, D. Methods of integrating data
458 to uncover genotype-phenotype interactions. *Nat. Rev. Genet.* **16**, 85–97 (2015).

459 6. Malik, V., Kalakoti, Y. & Sundar, D. Deep learning assisted multi-omics integration for survival
460 and drug-response prediction in breast cancer. *BMC Genomics* **22**, 1–11 (2021).

461 7. Singh, A. *et al.* DIABLO: An integrative approach for identifying key molecular drivers from
462 multi-omics assays. *Bioinformatics* **35**, 3055–3062 (2019).

463 8. Bersanelli, M. *et al.* Methods for the integration of multi-omics data: Mathematical aspects. *BMC
464 Bioinformatics* **17**, (2016).

465 9. Van Rooij, J. *et al.* Evaluation of commonly used analysis strategies for epigenome- A nd
466 transcriptome-wide association studies through replication of large-scale population studies.
467 *Genome Biol.* **20**, 1–15 (2019).

468 10. Litjens, G. *et al.* A survey on deep learning in medical image analysis. *Med. Image Anal.* **42**, 60–88
469 (2017).

470 11. Young, T., Hazarika, D., Poria, S. & Cambria, E. Recent trends in deep learning based natural
471 language processing. *ieee Comput. Intell. Mag.* **13**, 55–75 (2018).

472 12. Jumper, J. *et al.* Highly accurate protein structure prediction with AlphaFold. *Nature* **596**, 583–589
473 (2021).

474 13. Michael, K. Y. *et al.* Visible machine learning for biomedicine. *Cell* **173**, 1562–1565 (2018).

475 14. Bourgeais, V., Zehraoui, F., Ben Hamdoune, M. & Hanczar, B. Deep GONet: self-explainable
476 deep neural network based on Gene Ontology for phenotype prediction from gene expression data.
477 *BMC Bioinformatics* **22**, 1–24 (2021).

478 15. Ma, J. *et al.* Using deep learning to model the hierarchical structure and function of a cell. *Nat.
479 Methods* **15**, 290–298 (2018).

480 16. Wang, D. *et al.* Comprehensive functional genomic resource and integrative model for the human
481 brain. *Science (80-.).* **362**, eaat8464 (2018).

482 17. Moon, S. & Lee, H. MOMA: a multi-task attention learning algorithm for multi-omics data
483 interpretation and classification. *Bioinformatics* 1–10 (2022) doi:10.1093/bioinformatics/btac080.

484 18. van Hiltén, A. *et al.* GenNet framework: interpretable deep learning for predicting phenotypes
485 from genetic data. *Commun. Biol.* **4**, 1–9 (2021).

486 19. Elmarakeby, H. A. *et al.* Biologically informed deep neural network for prostate cancer discovery.
487 *Nature* **598**, 348–352 (2021).

488 20. Hao, J., Kim, Y., Kim, T. K. & Kang, M. PASNet: Pathway-associated sparse deep neural network
489 for prognosis prediction from high-throughput data. *BMC Bioinformatics* **19**, 1–13 (2018).

490 21. Kuenzi, B. M. *et al.* Predicting Drug Response and Synergy Using a Deep Learning Model of
491 Human Cancer Cells. *Cancer Cell* **38**, 672–684.e6 (2020).

492 22. Huang, X. *et al.* ParsVNN: Parsimony visible neural networks for uncovering cancer-specific and
493 drug-sensitive genes and pathways. *NAR Genomics Bioinforma.* **3**, 1–12 (2021).

494 23. Hannum, G. *et al.* Genome-wide Methylation Profiles Reveal Quantitative Views of Human Aging
495 Rates. *Mol. Cell* **49**, 359–367 (2013).

496 24. Horvath, S. *DNA methylation age of human tissues and cell types*. *Genome Biology* vol. 14
497 <http://genomebiology.com/14/10/R115> (2013).

498 25. Bell, C. G. *et al.* DNA methylation aging clocks: Challenges and recommendations. *Genome
499 Biology* vol. 20 (2019).

500 26. Langdon, R. J., Yousefi, P., Relton, C. L. & Suderman, M. J. Epigenetic modelling of former,
501 current and never smokers. *Clin. Epigenetics* **13**, (2021).

502 27. Maas, S. C. E. *et al.* Validated inference of smoking habits from blood with a finite DNA
503 methylation marker set. *Eur. J. Epidemiol.* **34**, 1055–1074 (2019).

504 28. Epigenetics of Lipid Phenotypes _ Enhanced Reader.pdf.

505 29. Zhernakova, D. V. *et al.* Identification of context-dependent expression quantitative trait loci in
506 whole blood. *Nat. Genet.* **49**, 139–145 (2017).

507 30. Bonder, M. J. *et al.* Disease variants alter transcription factor levels and methylation of their
508 binding sites. *Nat. Genet.* **49**, 131–138 (2017).

509 31. van Iterson, Maarten. Cats, D. Mei, L. BBMRIomics: R utilities for BBMRI omics data analysis; R
510 package version 3.4.2. (2020).

511 32. McLean, C. Y. *et al.* GREAT improves functional interpretation of cis-regulatory regions. *Nature
512 Biotechnology* vol. 28 495–501 (2010).

513 33. Kanehisa, M. & Goto, S. KEGG: kyoto encyclopedia of genes and genomes. *Nucleic Acids Res.*
514 **28**, 27–30 (2000).

515 34. Kamburov, A., Wierling, C., Lehrach, H. & Herwig, R. ConsensusPathDB - A database for
516 integrating human functional interaction networks. *Nucleic Acids Res.* **37**, (2009).

517 35. Jolliffe, I. T. Principal Component Analysis for Special Types of Data. 199–222 (1986)
518 doi:10.1007/978-1-4757-1904-8_11.

519 36. Ligthart, S. *et al.* Tobacco smoking is associated with DNA methylation of diabetes susceptibility
520 genes. 998–1006 (2016) doi:10.1007/s00125-016-3872-0.

521 37. Baiju, N., Sandanger, T. M., Sætrom, P. & Nøst, T. H. Gene expression in blood reflects smoking
522 exposure among cancer - free women in the Norwegian Women and Cancer (NOWAC)
523 postgenome cohort. *Sci. Rep.* 1–13 (2021) doi:10.1038/s41598-020-80158-8.

524 38. Vink, J. M. *et al.* Differential gene expression patterns between smokers and non-smokers : cause
525 or consequence ? 550–560 (2015) doi:10.1111/adb.12322.

526 39. Silva, C. P. & Kamens, H. M. Cigarette smoke-induced alterations in blood: A review of research
527 on DNA methylation and gene expression. *Exp. Clin. Psychopharmacol.* **29**, 116–135 (2021).

528 40. Kõks, S. & Kõks, G. Activation of GPR15 and its involvement in the biological effects of
529 smoking. *Experimental Biology and Medicine* vol. 242 1207–1212 (2017).

530 41. Braun, K. V. E. *et al.* Epigenome-wide association study (EWAS) on lipids: the Rotterdam Study.
531 *Clin. Epigenetics* **9**, 1–11 (2017).

532 42. Dekkers, K. F. *et al.* Blood lipids influence DNA methylation in circulating cells. *Genome Biol.* 1–
533 12 (2016) doi:10.1186/s13059-016-1000-6.

534 43. Srivastava, N., Hinton, G., Krizhevsky, A., Sutskever, I. & Salakhutdinov, R. Dropout: A simple
535 way to prevent neural networks from overfitting. *J. Mach. Learn. Res.* **15**, 1929–1958 (2014).

536 44. Davis, C. A. *et al.* The Encyclopedia of DNA elements (ENCODE): Data portal update. *Nucleic
537 Acids Res.* **46**, D794–D801 (2018).

538

539 Data availability

540 BIOS datasets are available from the European Genome-Phenome Archive by accession number
541 EGAS00001001077 (<https://ega-archive.org/studies/EGAS00001001077>). Alternative options to access
542 the data are available through the BIOS website; <https://www.bbmri.nl/acquisition-use-analyze/bios/>. All
543 trained networks are available on request.

544 Code availability

545 Code is available on GitHub: <https://github.com/ArnovanHilten/GenNet-multi-omic>

546 Acknowledgements

547 This work was funded by the Dutch Technology Foundation (STW) through the 2005 Simon Steven
548 Meester grant 2015 to W.J. Niessen. G.V. Roshchupkin supported by the ZonMw Veni grant (Veni,
549 1936320). The Rotterdam study is supported by the Netherlands Organization for Scientific Research

550 (NWO, 91203014, 175.010.2005.011, 91103012). This research was financially supported by BBMRI-
551 NL, a Research Infrastructure financed by the Dutch government (NWO, numbers 184.021.007 and
552 184.033.111). Samples used in this study were contributed by LifeLines, the Leiden Longevity Study, the
553 Netherlands Twin Registry (NTR) and the Rotterdam Study. This work was carried out on the Dutch
554 national e-infrastructure with the support of SURF Cooperative. We thank all participants and
555 investigators for their contributions to this study.

556 Contributions

557 A.H., J.v.R. and G.R. conceived and designed the method. A.H. performed experiments and implemented
558 the method. G.R., W.N. and J.v.M supervised the work. Data set generation and quality control of the
559 BIOS datasets was done by the BIOS Consortium, more details can be found at:
560 <http://www.bbmri.nl/acquisition-use-analyze/bios/>, including details on contributions of all consortium
561 members. A.H., J.v.R, G.R., A.I., W.N., and J.v.M wrote, revised, and approved the paper.

562 Competing interests

563 W. N. is co-founder and shareholder of Quantib BV. Other authors declare no competing interests.

564 Correspondence

565 Correspondence to a.vanhilten@erasmusmc.nl, g.roshchupkin@erasmusmc.nl

566